Unusual behavior of projectile fragments produced by the interactions of relativistic Ar ions with copper

K. Aleklett,[a] R. Brandt,[b] G. Dersch,[b] G. Feige,[b],[c] E. M. Friedlander,[c] E. Ganssauge,[d] G. Haase,[b] D. C. Hoffman,[c] J. Herrmann,[e] B. Judek,[f] W. Loveland,[g] P. L. McGaughey,[c],[h] N. T. Porile,[e] W. Shulz,[d] and G. T. Seaborg[c]

[a]*The Studsvik Science Research Laboratory, S-61182 Nyköping, Sweden*
[b]*Kernchemie, Philipps-Universität, D-3550 Marburg, Federal Republic of Germany*
[c]*Nuclear Science Division, Lawrence Berkeley Laboratory, Berkeley, California 94720*
[d]*Fachbereich Physik, Philipps-Universität, D-3550 Marburg, Federal Republic of Germany*
[e]*Department of Chemistry, Purdue University, West Lafayette, Indiana 47907*
[f]*High Energy Physics Section, National Research Council, Ottawa, Canada K1A 0R6*
[g]*Department of Chemistry, Oregon State University, Corvallis, Oregon 97331*
[h]*Los Alamos National Laboratory, Los Alamos, New Mexico 87545*

(Received 31 August 1987)

Radiochemical activation techniques were used to study the behavior of projectile fragments formed in the interaction of 0.9 A and 1.8 A GeV ^{40}Ar ions within thick Cu targets. Two identical 1 cm thick Cu disks were irradiated with separations between the disks of 0, 10, and 20 cm, respectively. The results show an enhancement in the formation of light mass ($A < 30$) radioactive residues in the second disk relative to the first in the contact configuration for both projectile energies. This enhancement decreases for increasing distance between the Cu disks. While our results with 0.9 A GeV projectiles can be explained within the framework of conventional nuclear physics, the data at 1.8 A GeV demand that either secondaries of $Z = 1$, neutrons and/or pions are emitted with surprisingly large transverse momenta, or that some projectile fragments have large interaction cross sections but decay in flight ($\tau \sim 10^{-10}$ s).

I. INTRODUCTION

Observations reporting the formation of projectile fragments with anomalously short mean field paths in relativistic heavy-ion collisions[1] have attracted considerable interest in recent years. This short mean free path of secondary fragments could not be explained within the framework of conventional nuclear physics. However, the effect itself has not been definitely established experimentally.[1–14] A large number of different experiments have been presented at the 1984 heavy ion study held at the Gesellschaft für Schwerenionenforschung and summarized by Heinrich *et al.*[14] In some experiments using the nuclear emulsion technique the anomalous behavior is observed while in others it is not. The same holds for experiments using CR-39 solid state track detectors. The early results from large counter experiments, which detect interactions via changes in the charge Z of projectile fragments with $8 \leq Z \leq Z_{\text{primary}}$, gave no evidence for anomalous projectile behavior. These results[9,10] were based on data sets with considerably higher statistics than those obtained by visual methods; their results, however, apply only to projectile fragments whose interactions lead to $\Delta Z \geq 1$ (i.e., a charge change of at least one unit between an incident heavy ion and its secondary heavy projectile fragment) moving within a narrow forward cone of $\simeq 3°$. A recent experiment using the same technique with higher spatial resolution[13] reports, however, a positive result. Bubble chamber experiments performed at the Joint Institute for Nuclear Research (JINR) accelerator[4,12] show with high statistics some striking evidence for anomalous behavior. In particular, Gasparian *et al.*[4] were able to show that for interactions of 4.1 A GeV ^{12}C in a propane bubble chamber one could observe a very strong short mean free path effect for primary interactions, in which $\Delta Z = 0$. In reactions with $\Delta Z > 0$, no such anomalously short mean free path could be observed. This was shown convincingly for reactions with $\Delta Z = 1$. Thus, from an experimental point of view, one has to consider the question of anomalously short mean free paths as being open. Consequently, it is important that as many different techniques as possible be brought to bear on this problem.

We report here the results of experiments in which *radiochemical activation techniques* have been used to search for the possible formation, interaction and decay of anomalous projectile fragments.

In these experiments, thick copper disks are exposed to a high fluence of relativistic heavy ions. Certain specific radioactive residues are produced in the interaction of the beam ions and their secondaries with the disk; these are identified by off line γ-ray spectroscopy. A typical example of such a radioactive nucleus is ^{24}Na ($T_{1/2} = 15.02$ h), which can easily be identified by its 1368.5 keV γ ray. Given a sufficiently high beam intensity of primary heavy ions, we can measure the ^{24}Na activity quite precisely ($\pm 1\%$). Comparable precision is obtained for a few similar nuclides. The specific reasons for our special interest in this nuclide will be given in detail in Sec. III.

Our radiochemical experimental technique is comple-

mentary to the other techniques used so far, in that we study the targetlike fragments of the interactions rather than the projectile fragments themselves. It also differs from them in two respects, namely (a) it is a global search for anomalous behavior of *any fast secondary;* (b) it looks at *partial* rather that at *total* cross sections.

These differences obviously entail advantages and disadvantages, which are given as follows:

(i) Advantages:

(a) Because of the high beam fluxes tolerated, the statistical accuracy greatly exceeds that of visual methods, and is comparable to that of direct counter measurements on secondaries.

(b) The search encompasses both charged and neutral secondaries, and charged pions as well as nuclear fragments.

(c) It covers in angle the *whole* fragmentation cone, and the pion and "participating nucleon" cone up to 20°.

(d) Because of the high threshold for the production of ^{24}Na, study of the production of ^{24}Na selects interactions induced by fast secondaries and not by slow, low energy secondaries, such as target fragments.

(e) Even if anomalous secondaries either do not exist, or do not contribute to the investigated partial cross section, this method provides a new measure for secondary energy flow (in a way, a new technique of calorimetry), and may implicitly reveal interesting features of the reaction mechanism.

(ii) Disadvantages:

(a) Any interesting effects may just happen to be absent in the *particular partial cross section(s) investigated.*

(b) The sensitivity to *all* kinds of fast secondaries may drown out an existing effect *if it happens to be localized in some special and rare subset.*

(c) Hence, a *null* effect may be inconclusive.

The experimental techniques used are described in Sec. II and the results in Sec. III. The interpretation of our experimental results described in Sec. IV is by necessity somewhat involved, since we do not directly observe the projectile fragments but only the products of their interactions. Partial results of this experiment were presented previously.[15]

II. EXPERIMENT

We carried out the experiments at the Bevalac [Lawrence Berkeley Laboratory, University of California, Berkeley (LBL)] using argon beams with 1.8 and 0.9 A GeV energy, respectively. At each of these energies a main experiment with Cu targets using activation techniques as well as an auxillary experiment using nuclear emulsion targets and visual techniques were carried out.

A. The copper experiment

The principle of our experiment is illustrated in Fig. 1. Two 1 cm thick circular copper disks ($r=4$ cm) were irradiated by the Ar beam (Fig. 1). In a typical irradiation, $\approx 10^{12}$ Ar ions passed through the Cu disks in a period of 2–4 h. The beam was well focused (nominal diameter

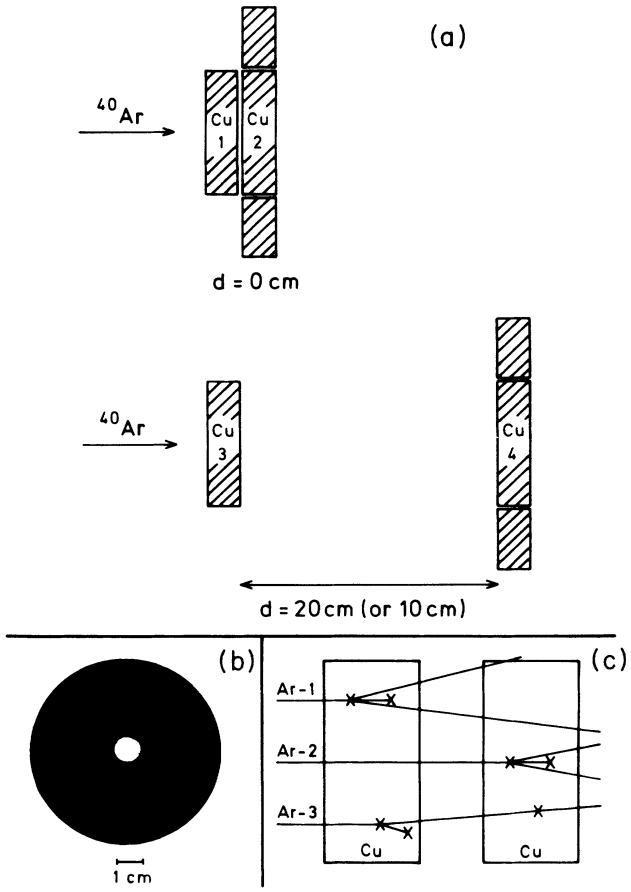

FIG. 1. (a) Schematic representation of the target setup using Cu disks and their surrounding guard rings. (b) Autoradiographic picture of a Cu disk after the irradiation. (c) Schematic representation of different reaction paths in the two Cu disks; details are given in text.

≈ 1 cm). As can be seen in an autoradiographic picture of an irradiated Cu disk [Fig. 1(b)], 99% of the beam was centered within an area of $r \leq 2$ cm. These autoradiographic pictures showed no significant difference for Cu disks numbered 1–4 [Fig. 1(a)]. For a given energy, pairs of Cu disks were irradiated together in a "contact" configuration ($d=0$ cm), with a separation of 10 cm, and a separation of 20 cm. In the contact configuration and in the $d=20$ cm configuration, the downstream Cu disks were surrounded by a 1 cm thick Cu guard ring ($r_{\text{out}}=7$ cm, $r_{\text{in}}=4$ cm) [Fig. 1(a)]. Both Cu disks in a particular configuration serve as targets for the primary beam, as well as for secondaries interacting within the same disk in which they were produced [trajectories Ar-1 and Ar-2 on Fig. 1(c)]. However, secondaries produced in the first disk (the "target" disk) and interacting in the second disk [the "detector" disk, trajectory Ar-3 in Fig. 1(c)] will enhance nuclide production in the "detector" disk. This enhancement may be especially strong if, among other reasons, such a projectile fragment has an unexpectedly high interaction cross section, i.e., a "too short" mean

free path.

After the completion of the irradiation, short-lived activities were allowed to decay for approximately 12–24 h. Afterwards, the radionuclides present in the irradiated Cu disks and guard rings were assayed by off-line gamma ray spectroscopy. The guard rings were cut into sections and reassembled to simulate the disk geometry for counting. Measurements were made with Ge(Li) detectors (resolution ~ 1.8 keV). The analysis of the γ-ray spectra was based on standard radiochemical procedures.[16] Counting was carried out for approximately one week at LBL and was continued for several months at Marburg. Independent determinations of most of the radionuclides present in each disk were made at LBL, Purdue, and Marburg and the whole experiment was repeated. All the results agreed with experimental uncertainties and the values from the different laboratories were averaged to give the final results. The experimental details have been described elsewhere.[17] Possible differences in counting efficiencies due to sample geometry were evaluated using homogeneous ^{24}Na sources produced by the ^{27}Al(n,α) reaction. We compared the counting efficiency of a point source (area ~ 1.5 cm^2) of ^{24}Na in ^{27}Al with a clearly exaggerated two-component source of ^{24}Na in ^{27}Al (70% within an area of 1.5 cm^2 and 30% homogeneously distributed over an area of 30 cm^2) in our typical counting configuration (source-detector distance $=8$ cm). This two-component source should simulate the slight beam blowup in downstream Cu disks [disk No. 2 and No. 4 in Fig. 1(a)]. The difference in counting efficiency between these two sample geometries was determined to be $(2\pm 1)\%$.[17,18] As a matter of fact, our beam spot was concentrated within an area considerably smaller than that of the test arrangement described above.

We determined the ratio R_d of the activity in the downstream disk to that in the upstream disk as a function of disk separation d, for specific nuclides within a pair of Cu disks. Because each pair of Cu disks was irradiated with the same particle beam simultaneously and assayed later for its gamma activity in a fixed position with the same Ge(Li) gamma detector, this measured activity ratio for a specific nuclide can be determined to a high degree of precision. All uncertainties due to particle fluxes, counting efficiencies, uncertainties in the decay scheme for a specific radioactive nuclide, etc. cancel out in the *activity ratios R*. Essentially, the only experimental uncertainty in this ratio comes from counting statistics. As the number of counts is typically $>10^4$ our activity ratio R can be determined within $\pm 1\%$. Such a precision is comparable only to that of large counter experiments or of high statistics bubble chamber experiments, as mentioned in the Introduction.

B. The emulsion experiment

When we attempted to predict [by means of Monte Carlo (MC) calculations based upon conventional high-energy nuclear physics] the contributions of different secondaries to the ^{24}Na (and similar) activities in the different disks, we were stymied by an unfortunate lack of detailed emulsion data concerning the multiplicity and angular distributions of secondaries from collisions of ^{40}Ar projectiles at 0.9 and 1.8 A GeV. Therefore a special emulsion investigation was found necessary as part of the present effort, to provide the necessary input data for our calculations. It was carried out in Ottawa and it is described below; its main results are presented in Table III. Detailed angular distributions measured in the same experiment are then presented and used in Tables V and VI.

A stack of Ilford G5 nuclear emulsions $10\times 20\times 0.06$ cm^3 each, exposed to the 1.8 A GeV argon beam of the Berkeley Bevalac was scanned along the track for Ar interactions both at the maximum (beam) energy and at a residual range where the beam was slowed down to about 0.9 A GeV. The secondary particles were classified as usual into "heavy" (N_h) tracks (mainly slow, target-related fragments), fast ($\beta > 0.7$)$Z=1$ "shower tracks" (n_s) and $Z>1$ projectile fragments (PF). "Shower tracks" can be pions ($E_\pi > 56$ MeV) or protons ($E_p > 375$ MeV). Among the PF's most α particles were identified by their specific ionization (α is hereafter a shorthand for all He isotopes). The charges of heavier fragments ($Z>2$) were visually estimated and the fragments classified into "light" ($\langle Z\rangle \approx 4$), "medium" ($\langle Z\rangle \approx 8$), "heavy" ($\langle Z\rangle \approx 16$), and "beamlike" ($Z=18$) PF's. Emission angles of all fast secondaries (i.e., shower tracks and PF) were measured with the high accuracy characteristic of the nuclear emulsion detector (i.e., to better than 0.1 deg). Fifty-six events were recorded at a projectile energy of 0.9 A GeV and 95 at 1.8 A GeV. These events gave rise to a total of 542 and 1178 fast secondaries, respectively, which were used as input for the subsequent MC calculation.

III. RESULTS

A. The copper experiment

We show (in Fig. 2) the dependence of R_d on the product mass number for two different separations ($d=0$ cm, $d=20$ cm) of the disks for reactions induced by 0.9 A GeV ^{40}Ar ions. The dependence of R_d on A is a reflection of the energy spectrum and angular distribution of the secondaries inducing reactions in the disks. The results for the 0.9 A GeV ^{40}Ar projectiles show that when the two disks are in contact (R_0), the projectile fragments (PF) most likely to strike the detector disk lead to the formation (by target fragmentation) of products with $A \simeq 55$ and substantial yields are seen for all products with $A>40$. The products with $A<30$ (^{7}Be,^{22}Na,^{24}Na,^{28}Mg) are formed only in high deposition-energy target fragmentation events.[20] They cannot be projectile fragments because these are much too energetic to stop in the copper disks.

When the disks are moved 20 cm apart, the "detector" disk samples a different subset of the PF created in the "target" disk, i.e. the more strongly forward focused and thus higher-energy fragments. As a result, the PF most likely to reach the second disk now lead to the formation of products with $A \simeq 45$ and the formation of heavier

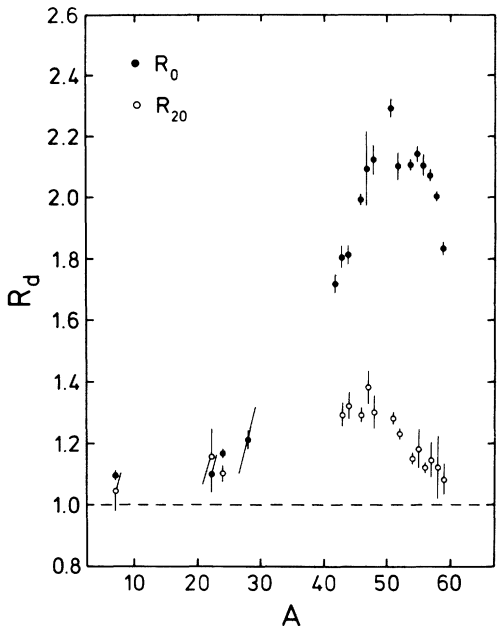

FIG. 2. Dependence of R_d upon product mass number for the interaction of 0.9 A GeV ^{40}Ar with Cu. Values for two disk separations, $d=0$ cm and $d=20$ cm, are shown.

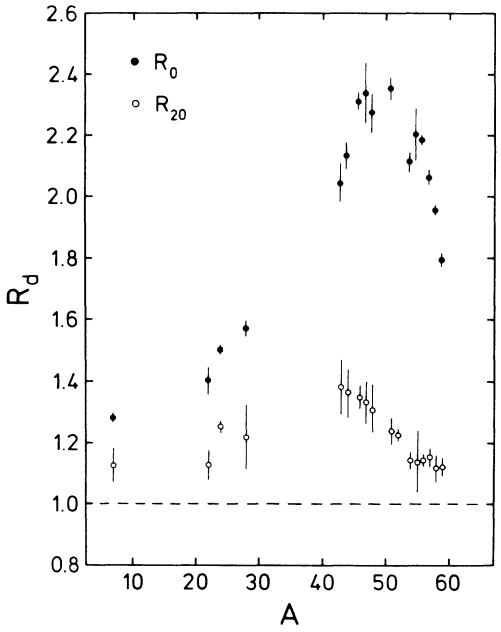

FIG. 3. Dependence of R_d upon product mass number for the interaction of 1.8 A GeV ^{40}Ar with Cu.

fragments is less likely. Not surprisingly, R_0 for these products is larger than R_{20} reflecting production by low-energy, wide-angle secondaries. The fragments with $A<30$ are produced with about the same yields regardless of disk separation because they are only produced by highly forward focused, energetic projectile fragments.

For the 1.8 A GeV ^{40}Ar beam, (Fig. 3) the dependence of R_0 on A for $A>40$ is similar to that obtained with 0.9 A GeV ^{40}Ar projectiles except for the shift of the most probable product mass number to a slightly lower value ($A\simeq 50$). The values of R_{20} (for $A>40$) are also similar to those obtained at 0.9A GeV. However, the results for products with $A<30$ are significantly different from those obtained with 0.9 A GeV ^{40}Ar. The values of R_0 are substantially higher, ranging from 1.3 to 1.6. Furthermore, the ratios decrease with separation between the disks, to values of R_{20} between 1.1 and 1.2

To emphasize the difference between measurements at $d=0$ cm and for $d=20$ cm, we show the ratio of cross section ratios

$$\rho=\frac{R(1.8A\ \text{GeV})}{R(0.9A\ \text{GeV})} \tag{1}$$

for $d=0$ cm in Fig. 4 (ρ_0) and for $d=20$ cm in Fig. 5 (ρ_{20}) for all the isotopes investigated. There is a sharp contrast between Figs. 4 and 5. It is interesting to note that ρ_0 has its maximum value (1.3) for low-mass products. All other ρ values are ≤ 1.15. This is another way of stating our experimental finding that something surprising is happening for low-mass fragments produced in the $d=0$ configuration by the 1.8 A Gev ^{40}Ar beam. The lowered ρ_0 value for ^{7}Be can be explained by noting that this nuclide is presumably produced via two different reaction mechanisms. Indeed ^{7}Be can be either the target residue of a very violent interaction (then its ρ value should be that of Na isotopes) or it is an evaporation product. In the latter case one would conjecture a ρ value close to unity, as observed for spallation products. As one would expect, a value intermediate between those extremes is observed.

We find that R values for ^{24}Na can be obtained more precisely than the corresponding R values for ^{7}Be, ^{22}Na, and ^{28}Mg under the conditions of our experiments. Accordingly, we focus our attention in the following discus-

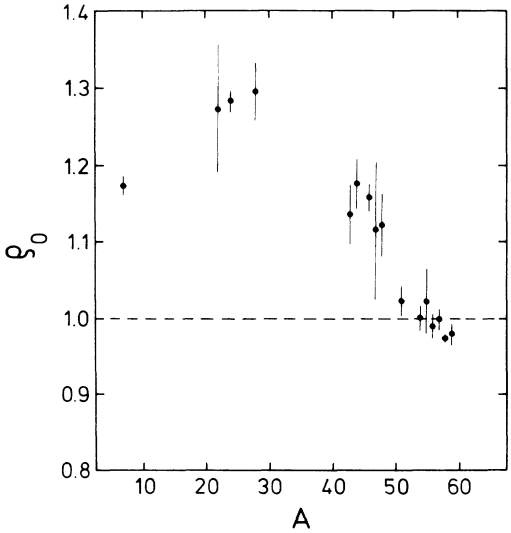

FIG. 4. Dependence of R_0 (1.8 A GeV)/R_0 (0.9 A GeV) upon product mass number.

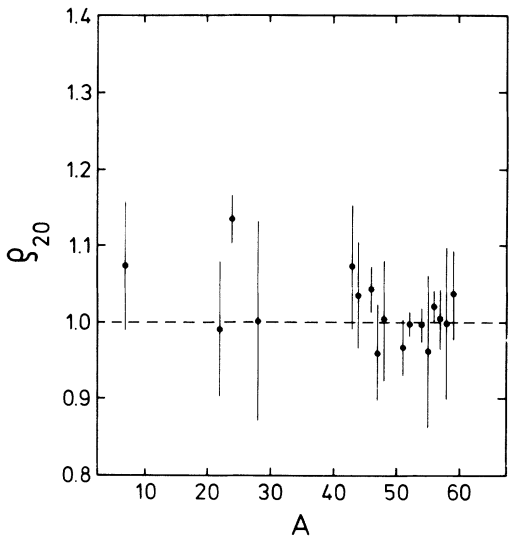

FIG. 5. Dependence of R_{20} (1.8A GeV)/R_{20} (0.9A GeV) upon product mass number.

sion to ^{24}Na, noting that all light residues (^{7}Be, ^{22}Na, ^{24}Na, and ^{28}Mg) behave similarily. We also note that the excitation function for ^{24}Na produced from Cu with high-energy particles is rather well known (Fig. 6); its steep rise between 1 and 2 GeV, and its subsequent saturation, turn our ("Cu target *cum* ^{24}Na seen") into a sort of "radiochemical threshold counter."

Numerical values of the ratios R_d for ^{24}Na are given in Table I. The results for the ratio of the ring activity to that of the downstream disk $R_{\text{ring},d}$ [No. 2, No. 4 in Fig. 1(a)] for specific radionuclides are given in Table II. The results for $d=0$, i.e., $R_{\text{ring},0}$ show that practically no high-energy particles hit this guard ring ($R_{\text{ring},0}<0.01$ for ^{24}Na) for reactions induced by either 0.9A GeV ^{24}Ar or 1.8A GeV ^{40}Ar. The results for $d=20$ cm, i.e., $R_{\text{ring},20}$, show that only a small fraction of high-energy secondary particles strike the guard ring, as we observe only $R_{\text{ring},20}=0.04$–0.07 at both ^{40}Ar beam energies for light products (e.g., ^{24}Na). However, we observe larger values of $R_{\text{ring},20}$ at both energies for spallation products close to the target (e.g., $R_{\text{ring},20}=0.17\pm0.01$ for ^{56}Co). The detailed discussion of the induced activity in the Cu disk and its surrounding guard ring for a separation of 20 cm is given in the next section. For $d=20$ cm the disk and the ring sample secondary fragments moving within a 11° cone and between 11° and 20°, respectively.

The results for ^{24}Na (Table I and Fig. 7) show a few interesting features: (i) a strong increase in R_0 when the Ar energy increases, (ii) R_d decreases slightly with d at 0.9A

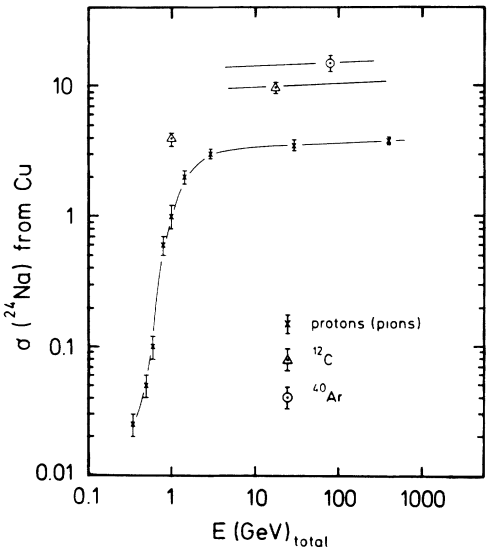

FIG. 6. Excitation function for the production of ^{24}Na from Cu using high energy projectiles (Refs. 16 and 18).

TABLE I. R_d values and derived quantities observed at the two beam energies.

	0.9A GeV ^{40}Ar	1.8A GeV ^{40}Ar
R_0[a]	1.167±0.011	1.501±0.008
R_{10}	1.118±0.020	1.373±0.034
R_{20}[a]	1.102±0.026	1.251±0.020
R_0/R_{10}	1.044±0.021	1.093±0.028
$R_0/(R_{20}+R_{\text{ring},20})$	1.019±0.025	1.120±0.019
$R_0-(R_{20}+R_{\text{ring},20})$	0.022±0.028	0.161±0.022

[a]The experiments determining R_0 were performed independently in triplicate, those for R_{20} in duplicate.

TABLE II. Relative yields of different nuclides in the upstream and downstream guard rings at the two beam energies.

	(a) 0.9A GeV ^{40}Ar	
Product	$R_{\text{ring},0}$	$R_{\text{ring},20}$
^{7}Be	<0.05	0.046±0.034
^{22}Na	<0.07	<0.07
^{24}Na	<0.01	0.039±0.002
^{28}Mg	<0.01	0.048±0.005
^{44m}Sc	0.009±0.002	0.124±0.006
^{46}Sc	<0.02	0.140±0.009
^{54}Mn	0.029±0.003	0.167±0.007
^{56}Co	0.027±0.005	0.166±0.008
^{58}Co	0.054±0.003	0.163±0.006
	(b) 1.8A GeV ^{40}Ar	
Product	$R_{\text{ring},0}$	$R_{\text{ring},20}$
^{7}Be	<0.02	0.072±0.013
^{22}Na	<0.03	<0.08
^{24}Na	<0.01	0.071±0.005
^{28}Mg	<0.01	0.060±0.010
^{44m}Se	0.012±0.001	0.134±0.008
^{46}Sc	0.015±0.003	0.159±0.007
^{54}Mn	0.041±0.002	0.174±0.007
^{56}Co	0.054±0.003	0.169±0.007
^{58}Co	0.065±0.003	0.168±0.006

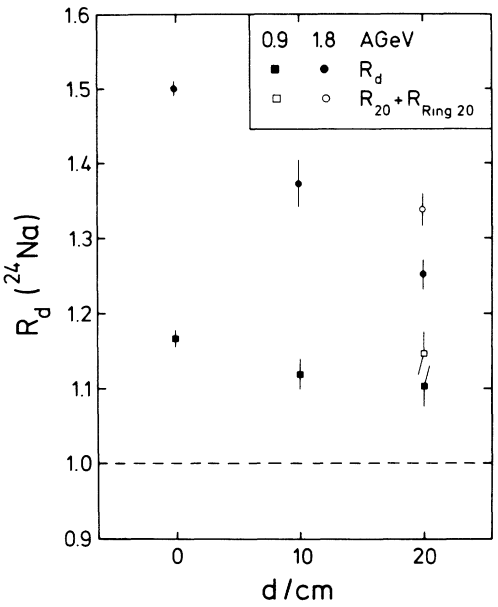

FIG. 7. Activity ratios R_d for ^{24}Na produced in Cu disks with relativistic Ar ions (where d is the distance between a pair of Cu disks).

GeV, but strongly at 1.8 A GeV. (iii) If we add the activity in the guard ring to that in the downstream Cu disk, this decrease is canceled at 0.9 A GeV, *but not at* 1.8 A GeV. These changes can be expressed quantitatively by comparing values of

$$X_{d,j}(0001) \equiv 100(R^*_{d,j}-1) , \tag{2}$$

i.e., of the deviation from unity of "corrected" ratios R^*_d; these are defined analogously to the R_d but with the activity of the guard rings *added* to that of the "detector" disks so as to compensate for beam divergence over the longer flight path. The second subscript (j) refers to the projectile energy (viz. $j=1$ to 0.9 A GeV and $j=2$ to 1.8 A GeV) (Note that for $d=0$ the ring activity is so low that R^*_d and R_d practically coincide.)

Then

$$X_{0,2}-X_{0,1}=(33\pm2)\% \tag{3}$$

while

$$X_{0,2}-X_{20,2}=(18\pm2)\% . \tag{4}$$

This behavior will be examined in the next section, using the information available at present about the mechanism of relativistic heavy ion collisions.

B. The emulsion experiment

Table III shows the main characteristics of the events observed at both energies for the well identified secondaries. Its last two rows present a few event characteristics based on the roughly estimated charges of PF's with $Z>2$. The first two columns in Table III refer to the total sample of events. It is well known that, on the average, nuclear emulsion behaves with respect to nuclear reactions like copper (e.g., the proton mean free path for nuclear collisions is 134 g/cm^2, as compared to 135 g/cm^2 in Cu). However the emulsion target nuclei are a mixture of light (C,N,O) and heavy (Ag,Br) targets. To define the possible range of parameters to be used in the MC calculations, the next four columns in Table III list the characteristics of events with $N_h \leq 8$ (corresponding mainly to nonperipheral collisions in CNO) and those with $N_h \geq 9$ (collisions with Ag and Br only, both of which are heavier targets than Cu). The mean number of target related fragments ($\langle N_h \rangle$) is approximately the same at the two energies as would be expected from limiting fragmentation. The mean number of shower tracks ($\langle n_s \rangle$) increases with beam energy by $\simeq 50\%$ as expected from increased pion production. The mean alpha particle multiplicity among the PF's decreases slightly (if at all) from 0.9 to 1.8 A GeV indicating perhaps a more thorough breakup of ^{40}Ar projectiles at the higher energy. The angular distribution of the shower tracks (as reflected in the mean emission angle) appears to be roughly the same at both beam energies whereas the alphas are more bundled at the higher energy (the same is true for the heavier PF's). This can be understood qualitatively by considering the line labeled $\langle n_s \rangle_{\theta<\theta_c}$ in Table

TABLE III. Mean characteristics of events induced by 0.9 A GeV and 1.8 A GeV ^{40}Ar projectiles in nuclear emulsion.

	All events		$N_h \leq 8$		$N_h \geq 9$	
	0.9 A GeV	1.8 A GeV	0.9 A GeV	1.8 A GeV	0.9 A GeV	1.8 A GeV
$\langle N_h \rangle$	10.8±1.5	9.8±1.5	3.8±0.5	3.0±0.3	23.8±0.8	22.6±1.6
$\langle n_s \rangle$	7.3±0.7	10.4±1.0	4.6±0.7	7.0±1.0	11.5±0.7	16.7±1.6
$\langle n_\alpha \rangle$	1.6±0.2	1.2±0.2	1.8±0.3	1.2±0.2	1.4±0.3	1.3±0.3
$\langle \theta^\circ_s \rangle$	16.8±0.8	16.7±0.5	12.5±1.0	14.0±0.7	19.5±1.1	18.8±0.7
$\langle \theta^\circ_\alpha \rangle$	2.5±0.2	1.9±0.1	2.2±0.2	1.7±0.2	3.1±0.3	2.2±0.2
θ°_c	10	6	10	6	10	6
$\langle n_s \rangle_{\theta<\theta_c}$	3.2±0.3	2.3±0.2	2.6±0.4	2.4±0.3	4.0±0.3	4.2±0.3
$\langle Z_F \rangle_{Z\geq 3}\rangle$	13	12	14	13	8	9
$\sum Z_{F,\theta<\theta_c}$	19	16	21	17	15	15

III, which shows the mean multiplicity of shower tracks in the "fragmentation cone" of the projectile, taken to be $\theta_c = 10°$ at $0.9A$ GeV and $\theta_c = 6°$ at $1.8A$ GeV. The numerical value for the critical angle θ_c has been derived *empirically* as described in Sec. IV B 1. These numbers suggest that the angular distribution of shower tracks at $1.8A$ GeV, which would be expected to be narrower than at $0.9A$ GeV because of the higher Lorentz factors involved, is widened by the particles lying beyond θ_c i.e., by the pions and the midrapidity protons. This is another hint of a somewhat more violent reaction mechanism at $1.8A$ GeV.

IV. PREDICTION OF ^{24}Na PRODUCTION

The results described in Sec. III suggest striking differences in the production behavior of the deep spallation products such as ^{24}Na produced by $0.9A$ GeV and $1.8A$ GeV, ^{40}Ar projectiles, namely (i) the significant increase of R_0 with projectile energy for Cu disks in contact (Table I and Fig. 4) and (ii) the decrease of R_d with distance d between the disks only at $1.8A$ GeV (Fig. 7).

Both results could be understood in terms of a relatively abundant production at the higher beam energy of projectile fragments with unexpectedly high interaction cross sections which "lose" this property ("decay") and revert to normal fragments after a flight path of the order of 20 cm. However, before drawing such a drastic and far reaching conclusion it is essential to investigate whether there exist other, possibly quite conventional, mechanisms capable of producing such a marked energy dependence.

We refer the reader again to Fig. 1(c). Because of the strong energy dependence of ^{24}Na production (Fig. 6), R_0 is sensitive to the multiplicities and the energy spectra of the secondaries (and, perhaps, slightly on the energy of the primary ^{40}Ar ion), whereas the variation of R_d with d is also dependent on their angular distribution. Indeed the simplest interpretation for effect 2), above, is that wide angle secondaries [illustrated by trajectory Ar-3 in Fig. 1(c)] miss the "detector" disk as well as its guard ring, *with the proviso* that their energy be sufficient (see Fig. 6) to ensure efficient ^{24}Na production. These two conditions can be fulfilled simultaneously *only if these secondaries have very large transverse momenta.* This would, by itself, be surprising because the whole experience with high-energy collisions has established that the *bulk* of secondaries have a *soft* transverse momentum spectrum.

In order to predict the R_d values one would ideally need a detailed Monte Carlo calculation of the *extra nuclear* cascade induced by the secondaries in the two Cu disks. For obvious reasons it is desirable that such a calculation be based as much as possible on *experimental facts* rather than on theoretical models. Unfortunately the ideal MC procedure would require a wealth of experimental input (a complete set of fragmentation cross section in copper for all possible reaction products together with their angular and momentum spectra) which is not available at present. In the following we shall adopt a mixed approach which (a) is based on the experimental information we obtained about multiplicities and angular distributions of secondaries from Ar interactions in nuclear emulsions, which simulate interactions in Cu rather well, and (b) makes exaggerated assumptions regarding the momentum spectra and the subsequent fate of the secondaries, in order to derive conservative estimates of the effects under consideration.

A. Estimation of effects in R_0

As indicated schematically in Fig. 1(c), R_0 is determined by five factors. All of these factors contribute to the total ^{24}Na activity observed in any given disk. These contributions (denoted hereafter by Q with an appropriate subscript) are expressed in terms of cross sections. Thus, e.g., for one interaction, $Q_{\mathrm{Ar}} = \sigma_{\mathrm{Ar}}$, where σ_{Ar} is the primary production cross section for the Cu(Ar,X) ^{24}Na reaction. The different contributions are: (i) beam interacting in disk 1 (Ar-1); (ii) beam surviving through disk one and interacting in disk 2 (Ar-2); (iii) secondaries from interactions in disk 1 (i.e., 1, above) interacting in the same disk; (iv) the same for disk 2 (i.e., 2 above); (5) secondaries emitted from interactions in disk 1 and interacting in disk 2 (Ar-3).

We denote by λ_{Ar} the collision mean free path (mfp) of the beam nuclei in Cu, by σ_{Ar} their cross section for producing ^{24}Na, by Q_{Ar} the total amount of ^{24}Na produced by primary ^{40}Ar in the first 1 cm Cu disk, by Q_{11} the total amount of ^{24}Na produced by all secondaries of type (iii) (together with their progeny in the extra-nuclear cascade) and by Q_{12} the same for secondaries of type (v). As defined above, Q_{Ar}, Q_{11}, and Q_{12} are expressed in terms of cross-section units.

Then the activities Q_1 and Q_2 of ^{24}Na produced in the two disks are given by

$$Q_1 \sim Q_{\mathrm{Ar}} + Q_{11} \,, \tag{5}$$

$$Q_2 \sim Q_1 e^{-x/\lambda_{\mathrm{Ar}}} + Q_{12} \tag{6}$$

[the latter, because the first term in Eq. (6) should be identical to Q_1 except for the attenuation of the beam in the first disk]. Thus

$$R_0 \equiv Q_2/Q_1 = e^{-x/\lambda_{\mathrm{Ar}}} + \frac{Q_{12}}{Q_{\mathrm{Ar}} + Q_{11}} \,, \tag{7}$$

where $x = 1$ cm is the disk thickness.

In the above equations the energy loss of both primaries and secondaries in the two copper disks have been deliberately ignored. Taking the energy loss into account could only *lower* (albeit slightly) the values of R_0.

Equation (7) can be qualitatively interpreted as follows: In zero-order approximation $Q_{12} \simeq 2Q_{11}$ because secondaries of type (v) traverse on the average twice the thickness of Cu traversed by those of type (iii) or (iv); in this approximation R_0 is determined essentially by the ratio Q_{11}/Q_{Ar}. Any increase in this ratio will increase R_0 up to a limiting value of $\simeq 2 + e^{-x/\lambda_{\mathrm{Ar}}}$ when $Q_{11} \to \infty$. If $Q_{11} \ll Q_{\mathrm{Ar}}$, then R_0 should drop below unity.

Note that *all* mfp's (primary as well as secondary) are considerably larger than x. Hence, to first order, one can approximate the (really exponential) distribution of beam interaction points in disk 1 by a uniform distribution. This places the average beam interaction at a depth $\approx x/2$ [a more rigorous calculation yields $(0.48-0.49)x$]. Thus, secondaries traverse in disk 2 roughly twice the thickness they had available in disk 1. This leads to

$$Q_{12} \approx 2Q_{11} \tag{8}$$

and hence

$$R_0 \approx e^{-x/\lambda_{\mathrm{Ar}}} + \frac{2}{1+Y} \tag{9}$$

where

$$Y \equiv \frac{Q_{\mathrm{Ar}}}{Q_{11}} \ . \tag{10}$$

In order to be independent of the *absolute* value of λ_{Ar} (which affects only the absolute value of R_0 and the absolute values of beam PF cross sections), we concentrate on the difference ΔR_0 between the R_0 values observed at 1.8 and 0.9 A GeV

$$\Delta R_0 = 2\left[\frac{1}{1+Y_{1.8}} - \frac{1}{1+Y_{0.9}}\right] \ . \tag{11}$$

Experimentally (see the first row of Table I):

$$\Delta R_{\mathrm{experimental}} = 0.334 \pm 0.014 \ . \tag{12}$$

The rest of this subsection is devoted to an intuitive, if somewhat simplified, calculation of Q_{11} aimed at checking whether the predicted value of ΔR_0 can be made to match the previously mentioned experimental value. A more sophisticated Monte Carlo (MC) calculation, *which leaves the main conclusion unchanged,* is briefly described in the Appendix.

At this stage it is important to point out that a thorough look at the definition of Q_{11}, and at the form of Eq. (11) allows one to avoid a seemingly obvious misinterpretation of the raw emulsion data. Indeed, we see in Table III that between beam energies of 0.9 A GeV and 1.8 A GeV $\langle n_s \rangle$ increases by $\approx 43\%$. This might lead to the *erroneous* conclusion that this increase is sufficient to justify the observed ΔR_0. However, (a) Q_{11} *includes* the energy dependence of cross sections, and (b) Eqs. (9) and (11) are *nonlinear* in Q_{11}, so that its effects are *weakened* in ΔR_0 (provided the Y ratios do not assume unreasonably *large* values).

This means that a *direct* comparison between ΔR_0 (and, incidentally, also R_0) and *numbers* of secondaries is not as straightforward as it seems.

In order to sort out the different components among the secondaries we note that there are two angular regions obeying *different* physics, i.e., the "fragmentation cone" ($\theta < \theta_c$) and the "midrapidity" region ($\theta > \theta_c$). The population of fast secondaries at very low rapidities (say, $\theta > 75°$) is at these beam energies practically extinct. The fragmentation cone contains as a rule (more precisely in $\sim 70\%$ of the cases) one heavy fragment ($Z \geq 3$), alphas and (p,d,t), with $n_p \gg n_d, n_t$. The latter angular region is populated by "midrapidity" protons and neutrons (coming mainly from the projectile and scattered outside the projectile fragmentation cone by interactions in the target) and by charged pions (these mainly at 1.8 A GeV). The delimiting angle θ_c separating these two angular regions comes from straightforward relativistic kinematics.

1. *The fragmentation cone*

Consider particles of mass m evaporated from some system moving with velocity β_{cms} (Lorentz factor γ_{cms}) with respect to the laboratory frame. Denote laboratory values for total and kinetic energies, momenta, velocities and angles by E, E_k, p, β, and θ, and corresponding quantities in the omitting (i.e., effective cms) system by primed symbols. The transverse and longitudinal components of p are denoted by $p_\perp$ and p_x. The laboratory emission angle θ is given by

$$\tan\theta = \frac{p_\perp}{p_x} = \frac{\sin\theta'}{\gamma_{\mathrm{cms}}(\mu + \cos\theta')} \tag{13}$$

where

$$\mu = \frac{\beta_{\mathrm{cms}}}{\beta'} \ . \tag{14}$$

For *heavy* particles which are *slow* in the emitting system $\mu \gg 1$:

$$\gamma_{\mathrm{cms}} \tan\theta \approx \frac{\beta' \sin\theta'}{\beta_{\mathrm{cms}}} \ . \tag{15}$$

This is indeed our case where e.g., alphas and nucleons are evaporated with temperatures between 5–20 MeV in the rest system of a residue of the argon projectile moving with beam velocity.

Since the θ are small, $\tan\theta \approx \theta$;

$$\gamma_{\mathrm{cms}}^2 \langle \theta^2 \rangle \approx \frac{\langle \beta'^2 \rangle \langle \sin^2\theta' \rangle}{\beta_{\mathrm{cms}}^2} \ . \tag{16}$$

Now for isotropic emission in the projectile frame

$$\langle \sin^2\theta' \rangle = \tfrac{2}{3} \ . \tag{17}$$

If thermal equilibrium prevails, then for two different kinds of particles of masses m_1 and m_2 the two *mean* kinetic energies are equal and the ratio of the two rms angles is

$$\frac{\theta_{\mathrm{rms},1}}{\theta_{\mathrm{rms},2}} = \left[\frac{m_2}{m_1}\right]^{1/2} \ . \tag{18}$$

In other words, the rms proton angle is twice the rms alpha angle.

For $\mu > 1$ (*which is always our case*) a maximum (or limiting) angle θ_c exists in the laboratory system, such that

$$\gamma_{\mathrm{cms}} \tan\theta_c = \frac{1}{(\mu^2 - 1)^{1/2}} \ . \tag{19}$$

Again, for $\mu \gg 1$,

$$\frac{\theta_{c,p}}{\theta_{c,\alpha}} = \frac{\mu_\alpha}{\mu_p} \approx 2 \ . \tag{20}$$

An exact MC calculation, taking into account the Boltzmann spectra of the evaporated particles, shows that without any approximations and for temperatures up to 40 MeV Eq. (20) is good to better than 5%. Hence, the recipe for determining θ_c *empirically* is to forget about the value of the temperature; search the emulsion data for the largest observed alpha emission angle; double that value and obtain θ_c i.e., the limit of the fragmentation cone (since the protons are the lightest fragments emitted).

2. *Angular region covered by "participating nucleons"*

Sorting our protons and pions *outside* the fragmentation cone does matter because at the same angle protons and pions will tend to have different energies, hence different cross-sections for producing ^{24}Na.

However, all fast particles ($\beta > 0.7$) of $Z = 1$ look alike in the emulsion (in terms of their track density, i.e., of their specific energy loss). A rough delimitation, (which tends to *exaggerate* ΔR_0) can be based on charge conservation. The total charge emitted into θ_c is given by

$$Z_c = Z_F + 2n_\alpha + n_{p,c} \ , \tag{21}$$

where Z_F is the charge of the heavy fragment and $n_{p,c}$ is that subset of the n_s ("fast" $Z = 1$, $\beta > 0.7$ secondaries) which are emitted with θ below θ_c. Since $Z_{\text{incident}} = 18$ we expect

$$\Delta Z = 18 - Z_c \tag{22}$$

protons (plus an equal number of neutrons) to be present beyond θ_c. The optimum conditions for ^{24}Na production (thus exaggerating our effect) obtain if we progress *outward* from θ_c and accept everything as protons until their sum has reached ΔZ. (In fact, some mesons reach into smaller angles as well, but this would only *lower* ^{24}Na production.)

From the observed alpha values we find that at $0.9A$ GeV $\theta_c \simeq 10°$ and at $1.8A$ GeV $\theta_c \simeq 6°$. The ratio of these angles lie close to the inverse ratio of the γ_{cms} values (1.959 and 2.919, respectively).

We see in Table III that, as one would expect, *there is no significant increase with energy of the multiplicity in the fragmentation cone,* where most of the ^{24}Na production must be concentrated (in view of the heavy PF's and their kinetic energies which entail large cross sections). *All* the increase in n_s is located *outside* θ_c where the energies and hence the cross sections are *small.* Obviously most, if not all, of this increase is due to pion production.

3. *Cross sections*

Now we have to assign cross sections to the different components as follows.

We assume that all projectile fragments with $A \geq 4$ have energy independent cross sections σ_F, and interpolate between the (saturation) proton (Ref. 19), carbon (Ref. 20), and argon (Ref. 17) values by a power law:

$$\sigma_F(A) \simeq 3.6 A^{0.387} \ . \tag{23}$$

For protons and pions we approximate the curve in Fig. 6 by

$$\sigma_p(E_k) = e^{-0.17 + 2.50u - 1.22u^2} \ , \tag{24}$$

where

$$u \equiv \ln E_k \tag{25}$$

if $E_k \leq 3$ GeV, and

$$\sigma_p(E_k) = 2.88 E_k^{0.0496} \tag{26}$$

otherwise. The E_k for the different components are obtained as follows:

(i) For the p,n in the fragmentation cone we note that the Lorentz transform reads

$$E = \gamma_{\text{cms}}(E' + \beta_{\text{cms}} p' \cos\theta') \ , \tag{27}$$

and since for any symmetric angular distribution in the rest frame $\langle \cos\theta' \rangle = 0$,

$$\langle E \rangle = \gamma_{\text{cms}} E' \tag{28}$$

which to first order reduces to

$$\langle E \rangle \simeq m \gamma_{\text{cms}} \ . \tag{29}$$

In other words, one should assign to these particles "beam velocity." This leads to $\sigma_p = 0.64$ mb at $0.9A$ GeV and to $\sigma_p = 2.24$ mb at $1.8A$ GeV. This is, however, an upper limit, because the (σ_p, E_k) relationship is highly nonlinear and

$$\langle f(x) \rangle \neq f(\langle x \rangle) \ ; \tag{30}$$

the inequality is always true; in our case substantially so. In order to see how much Eq. (30) may be in error, we have also done an MC calculation taking into account both the spreads in E' and in $\cos\theta'$; it turns out that the average cross sections are always *lower* than for "beam velocity." Thus, Eq. (29) is a *conservative* estimate.

(ii) For particles outside θ_c we use the streamer chamber results of Ref. 21. These tell us that in Ar + KCl "central" collisions at $1.8A$ GeV the transverse momentum distributions are of Boltzmann shape with "temperatures" T of 56 MeV for pions and 120 MeV for protons.

The shape of the transverse momentum spectrum has a quite dramatic effect on the cross section for producing ^{24}Na *at a given angle.* As an example, we illustrate in Fig. 8 the situation at an emission angle of 30° (secondaries which miss the downstream guard ring). The transverse momentum distribution, as well as that of kinetic energy, dies out long before the cross section has reached its saturation value.

So we have to average $\sigma_p(E_k(p_\perp, \theta))$ over the Boltzmann distribution between the limits

$$p_{\perp,\min} = p_{\min} \sin\theta \tag{31}$$

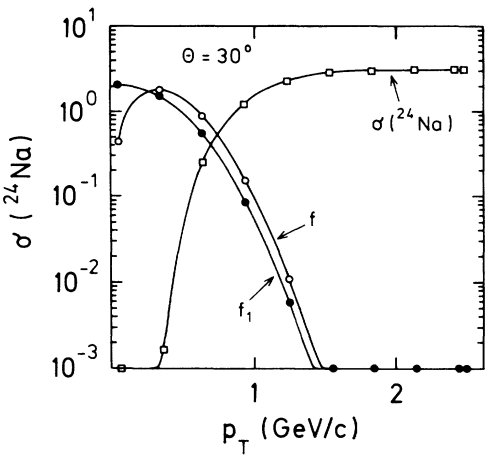

FIG. 8. Comparison between the transverse momentum distribution (open circles), the kinetic energy distribution (solid circles), and the ^{24}Na production cross section (open squares) for protons emitted at 30° to the beam. A Boltzmann spectrum with $T=120$ MeV was assumed for p_T.

with $p_{\min}$ computed for a given mass from $\beta \geq 0.7$ (i.e., the criterion for classifying the particle as "relativistic") and $p_{\perp,\max}$ resulting from

$$E_{\text{beam}} = \left[\frac{p_{\perp,\max}^2}{\sin^2\theta} + m^2 \right]^{1/2} \tag{32}$$

(energy conservation):

$$\langle \sigma \rangle = \frac{\int_{p\perp,\min}^{p\perp,\max} f(p_\perp)\sigma_p(E_k(p_\perp,\theta))dp_\perp}{\int_{p\perp,\min}^{p\perp,\max} f(p_\perp)dp_\perp} , \tag{33}$$

TABLE IV. Average cross sections (in mb) for the production of ^{24}Na by fast singly charged secondaries emitted at different angles (see text, Sec. IV A 3).

	Pions		Protons	
θ°	0.9A GeV	1.8A GeV	0.9A GeV	1.8A GeV
2.5	0.220	1.161	0.269	1.209
8.0	0.160	0.454	0.249	0.918
13.0	0.081	0.112	0.214	0.529
18.0	0.030	0.031	0.170	0.269
23.0	0.010	0.010	0.127	0.152
28.0	0.004	0.004	0.094	0.099
35.5	0.001	0.001	0.064	0.064
50.5	$\simeq 0$	$\simeq 0$	0.042	0.042
73.0	$\simeq 0$	$\simeq 0$	0.034	0.034

where

$$f(p_\perp) = \frac{p_\perp}{\omega^2} e^{-p_\perp^2/2\omega^2} , \tag{34}$$

$$\omega = \sqrt{mT} , \tag{35}$$

$$E_p(p_\perp,\theta) = \left[\frac{p_\perp^2}{\sin^2\theta} + m^2 - m \right]^{1/2} , \tag{36}$$

and σ_p is given by Eqs. (24)–(26).

The integration has to be carried out numerically; it leads to Table IV which gives, in mb, the average cross section for ^{24}Na production by pions and protons at a given angle θ (the center of the intervals used in Tables V and VI) and at the two beam energies. The energy dependence comes entirely from the upper integration limit, whereas the particle mass appears in both limits.

TABLE V. Schematic presentation of the factors contributing to Q_{11} (last column), using as input the "average emulsion event" at 0.9A GeV.

		$E_{\text{beam}}=0.9A$ GeV: 56 Events				
Secondary	Observed number	Mean number	Effective path	$\sigma(^{24}\text{Na})$ mb	Type	Effective ^{24}Na (mb)
Heavy fragments $Z \geq 3$	37	0.66	0.500	12.7	$Z \approx 13$	1073.7
α	92	1.64	0.500	6.16	α	746.2
$Z=1$ with θ°						
From To						
0 5	97	1.73	0.500	0.640	p,n	124.4
6 10	82	1.46	0.505	0.640	p,n	104.4
11 15	64	1.14	0.513	0.214	p,n	24.3
16 20	49	0.88	0.526	0.170	p,n	16.9
21 25	27	0.48	0.543	0.127	p,n	5.3
26 30	23	0.41	0.566	0.094	p,n	3.4
31 40	31	0.55	0.614	0.001	π	5.5
41 60	26	0.46	0.786	~ 0	π	3.2
61 85	11	0.20	1.710	~ 0	π	2.1
Total $Z=1$		7.31				289.5
Grand Total						2109.4

TABLE VI. Same as Table V, but at 1.8 A GeV.

Secondary	Observed number	$E_{beam}=1.8A$ GeV: 95 Events Mean number	Effective path	$\sigma(^{24}Na)$ mb	Type	Effective ^{24}Na (mb)
Heavy fragments $Z\geq 3$	73	0.77	0.500	12.3	$Z\approx 12$	2019.6
α	117	1.23	0.500	6.16	α	945.1
$Z=1$ with θ°						
From To						
0 5	250	2.63	0.500	2.240	p,n	1118.0
6 10	196	2.06	0.505	0.918	p,n	357.4
11 15	132	1.39	0.513	0.529	p,n	133.8
16 20	114	1.20	0.526	0.031	π	59.9
21 25	69	1.73	0.543	0.010	π	13.2
26 30	50	0.53	0.566	0.004	π	8.8
31 40	82	0.86	0.614	0.001	π	~0
41 60	69	0.73	0.786	~0	π	~0
61 85	24	0.25	0.710	~0	π	~0
Total $Z=1$		10.38				1691.1
Grand total						4655.8

4. *Computing Q_{11}*

What remains to be done now is to add all these contributions, properly weighted, into Q_{11}. The weights are products of the mean multiplicities ν_j of secondaries of a given kind and of the probability that they will interact in the residual disk thickness ($\approx x/2$).

Thus

$$Q_{11}=\sum_j \nu_j(1-e^{-x/2\lambda_j})\sigma_j \tag{37}$$

which reduces to

$$Q_{11}\approx \sum_j \nu_j \frac{x}{2\lambda_j}\sigma_j \ , \tag{38}$$

where j goes through *all* kinds of particles and angular intervals and λ_j is the interaction mfp of secondaries of type j.

Since for any given target material

$$\lambda_j\sigma_{t,j}=\text{const}=\lambda_p\sigma_{t,p} \ , \tag{39}$$

where the σ_t are total cross sections and the subscript p refers to protons (for which the mfp in Cu is known to be 15 cm), we get

$$Q_{11}\approx \sum_j \nu_j \frac{x}{2\lambda_p}\frac{\sigma_{t,j}}{\sigma_{t,p}}\sigma_j \ . \tag{40}$$

For the total cross section we use the geometrical (Bradt-Peters) formula

$$\sigma_{t,j}\simeq(A_j^{1/3}+A_{\text{Cu}}^{1/3}-b)^2 \tag{41}$$

from which we get the ratio of total cross sections:

$$\frac{\sigma_{t,j}}{\sigma_{t,p}}=\frac{(A_j^{1/3}+4-b)^2}{(5-b)^2} \ , \tag{42}$$

where the correction factor b lies close to unity (overlap $\simeq 1$ Fermi). We have done detailed calculations with b varying from 0.5 to 2 and they have brought no qualitative change in the data.

In order to visualize how the different components might add up into Q_{11} we give in Table V a schematic display of the structure of Q_{11}. Angular intervals have been compacted whenever necessary, in order to ensure reasonable statistics per interval (thus mean populations should be reduced correspondingly to yield a "readable" angular distribution.) The "π vs (p,n)" assignments are only symbolical, but the final results (the column labelled "effective ^{24}Na") are computed from the detailed data.

Actually the calculations have been performed separately for the five groups of events with either (a) no heavy fragments ($Z>2$) in the fragmentation cone ("Explosions"), or (b) with one fragment of mean (estimated) charge of either 4, 8, 16, or 18 (beamlike secondary fragment).

Obviously, in each group, the angular distributions are different, and thus the demarcation angle between "pions" and "nucleons" lies at a different values. All "nucleon" contributions to ^{24}Na production were doubled, in order to take account of neutrons. Table VII shows how the final result for ΔR_0 is reached.

Since the "average emulsion target" cannot be expected to be identical to the homogeneous ^{64}Cu target used in our experiments, we show in Table VIII the results of calculations using as input certain subsets of the emulsion events. They provide "bracketing" values meant to convey an idea of the extreme range of ΔR_0 values: (a) "Light" corresponds to events with mainly (C,N,O) target, i.e., $N_h\leq 8$; "heavy" means (Ag,Br), i.e., $N_h\geq 9$. (b) $Z_{\text{Frag}}=0$ symbolizes "explosions," i.e., relatively central collisions (in which the projectile is obliterated); $Z_{\text{Frag}}\geq 2$ are correspondingly more peripheral events. (c) The main values were computed for $b=1$; values in

TABLE VII. Factors contributing to the computed value of ΔR_0.

	0.9 A GeV	1.8 A GeV
Q_{Ar}(mb)	77.3	77.3
Q_{11}(mb)	37.7	49.0
Y	2.053	1.578
$\frac{2}{1+Y}$	0.655	0.776
ΔR_0	0.121	

parentheses correspond to the exaggerated assumption of $b=2$ (which would increase the weight of *large* total cross sections).

The values in parentheses are obtained by pushing the uncertain parameter b up to the extreme value of 2. All more realistic variations of parameters yield *lower* values of ΔR_0. Thus, for example, the only really meaningful (lower right-hand corner) element of the table drops to 0.092 if $b=0$ and a realistic evaporation temperature of 10 MeV is chosen.

In summary, we see that it is hard to bring the computed ΔR_0 into agreement with the experimental value [Eq. (12)] as long as one believes at all that the errors assigned to the R_0 values are correct.

In order to see what increases in the experimental errors would be necessary to reconcile the computed and experimental values we assume the (clearly exaggerated) value of $b=2$, and subtract the extreme ΔR_0 value (i.e., $\Delta R_0=0.141$) from the experimental one:

$$\Delta R_{\text{experimental}}-\Delta R^{\text{extreme}}_{\text{computed}}=0.193\ . \tag{43}$$

To reduce this difference to $\simeq 3$ standard deviations one would need an error in ΔR_{exper} of ≈ 0.064, i.e., *larger by a factor of almost 5 than the value obtained from experimental statistics.*

5. *Further cascading*

How often does this occur? Denote by ϵ the mean number of collisions of a particle (supposed "nondegradable") over some length x:

$$\epsilon=\frac{x}{\lambda}\ . \tag{44}$$

This mean includes obviously *all* traversals of x, including those with no collisions at all. The mean number ϵ_1 if at least one collision has occurred is then

$$\epsilon_1=\frac{\epsilon}{1-e^{-\epsilon}}\ ; \tag{45}$$

with $0.5\le x\le 1$ cm and $5\le\lambda\le 15$ cm, ϵ_1 is at worst 1.103, at best 1.017. Hence, tertiary, etc. collisions could account for something like a 5% increase in Q_{11}. This will then translate, as we know, nonlinearly, i.e., even more weakly, into ΔR_0.

How much does it contribute to the effect? The only way that a somewhat larger contribution of cascading could come about is if in a higher-order generation some of the heavy fragments blow up completely into their $\approx 2Z_F$ consistent nucleons which then have a chance to create further ^{24}Na. The extreme example for such a behavior is the first (i.e., left-hand) column in Table VIII, which derives from the total breakup of argon nuclei. This kind of effect would then have to be weighted by the small probability of tertiary interactions in our 1 cm thick disks. The Appendix explains how this effect was taken into account.

TABLE VIII. Computed values of ΔR_0 for different subsets of emulsion events (described in the text), assuming $b=1$ for the overlap parameter. Values in parentheses refer to an exaggerated value of $b=2$.

Target	$Z_{\text{frag}}=0$	$Z_{\text{frag}}>2$	All Z_{frag}
Light	0.111	0.075	0.066
	(0.127)	(0.089)	(0.077)
Heavy	0.236	0.123	0.179
	(0.277)	(0.144)	(0.209)
Emulsion	0.178	0.084	0.121
	(0.206)	(0.099)	(0.141)

B. Estimation of the "angular loss" outside the guard rings

Now we address the decrease of R_d at 1.8 A GeV as shown in Fig. 7. We remember that all PF ($Z>2$) are moving forward in a narrow cone, limited by $\theta_c=6°$. The dependence of ^{24}Na production by $Z=1$ secondaries on

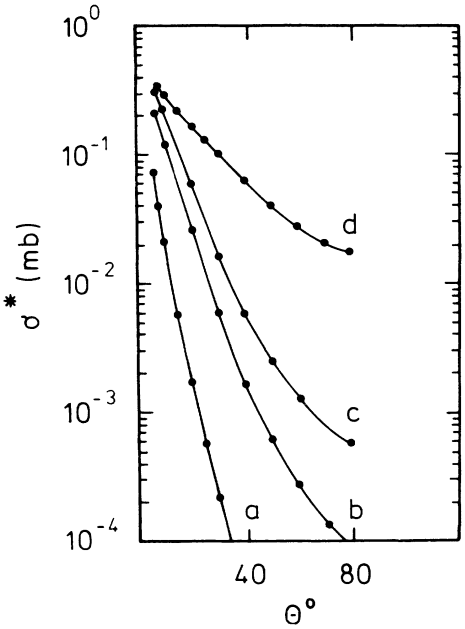

FIG. 9. Dependence of effective ^{24}Na production [σ^*/(mb)] by $Z=1$ particles on their emission angle in a 1 cm layer of Cu. Further details are given in the text. (a) refers to pions at $T=80$ MeV, (b)–(d) refer to protons with $T=120$, 400, and 800 MeV, respectively.

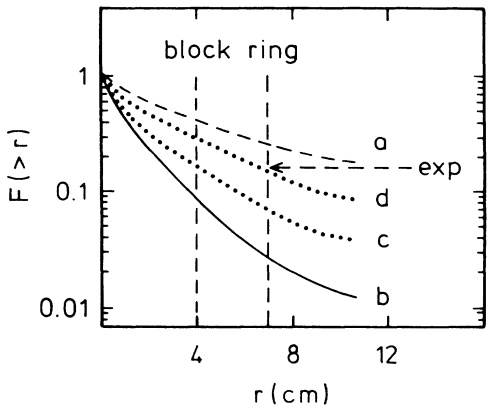

FIG. 10. (b)–(d)—Integral probability $F(>r)$ for the production of ^{24}Na by secondary particles beyond a radial distance r from the beam axis in a Cu block located at 20 cm from the source. The experimental integral angular distribution for $Z=1$ particles observed at $1.8A$ GeV ^{40}Ar in nuclear emulsions is shown (a) and was used for calculations, as described in the text. (b), (c), and (d) refer to protons emitted from a source with temperatures of $T=120$, 400, and 800 MeV, respectively.

their emission angle (outside the narrow fragmentation cone) in a layer of 1 cm Cu is given (in mb) in Fig. 9. The experimental setup was shown in Fig. 1: We have a 1 cm Cu disk as generator of secondaries and 20 cm downstream as 1 cm extended Cu plate. As input data we use the experimental angular distribution for $Z=1$ particles, as obtained from nuclear emulsions. The curves in Fig. 8 were obtained by averaging the cross sections at each angle over the (Boltzmann) transverse momentum spectrum, as described in Sec. VI B 3 Eqs. (31)–(36).

Extra-nuclear cascading was then taken into account as described in the Appendix. Curve a refers to pions while curves b–d refer to protons with temperatures of 120, 200, and 800 MeV, respectively. It is seen that in going from θ_c to 20° (the polar angle covered by the guard ring at $d=20$ cm) the effective pion cross section drops by a factor of ≈ 20; for protons at "reasonable" temperatures (100–200 MeV) the drop in cross section is still of 1 order of magnitude. Only quite exaggerated "equivalent temperatures" would be capable of conserving any sizable ^{24}Na production at and beyond 20°.

In Fig. 10 the dashed curve a shows the integral probability $F(>r)$ for a secondary to arrive at, or beyond a radial distance r from the beam axis in a Cu disk located at 20 cm from the source (at a beam energy of $1.8A$ GeV) for the angular distribution seen in the emulsion data. However, taking into account the weights due to the energy distribution of these particles, the full curve b then shows the integral ^{24}Na production by protons assuming 30% for the "blowup" probability P_b and an equivalent proton temperature $T_p=120$ MeV. Numerical values for results integrated over angles are given in Table IX. The dotted curves c and d are obtained by assuming exaggerated temperatures of 400 and 800 MeV, respectively.

The vertical dashed lines show the edges of the main Cu disk ($r=4$ cm) and of the guard ring ($r=7$ cm). The horizontal arrow shows the integral probability needed to reproduce the observed decrease in R_d with distance, which is one of the main puzzles resulting from this activation experiment. From Table X we see that it is possible to understand the "angular loss" outside the central ($r=4$ cm) Cu "disk" at $d=20$ cm for the $0.9A$ GeV beam; experimentally we observe $(6\pm3)\%$ of the total ^{24}Na activity outside the central "disk" and $(2\pm3)\%$ even outside the guard rings. Assuming a reasonable source temperature within the fireball of $T_p=120$ MeV and a 50% contribution of pions among the shower tracks (i.e., $P_p=0.5$) we can easily fit the experimentally observed values. However, at $1.8A$ GeV it seems to be impossible to obtain such a fit, except by assuming an absurdly high source temperature within the fireball ($T=800$ MeV), and only 10% of pions among the shower tracks. Even the relatively large amount of ^{24}Na found in the guard ring itself cannot be accounted for.

V. DISCUSSION

In order to see what kind of cross sections would be required for secondaries to reproduce the R_0 value at $1.8A$ GeV we added to the MC procedure the possibility that a fraction α of secondary projectile fragments ($Z\geq 3$) interact with a *total* cross section f times larger than the normal one. It turns out that in order to raise R_0 to ~ 1.5, it is sufficient to keep the product of α and f close to

$$\alpha f \simeq 2 , \tag{46}$$

(e.g., 10% secondaries with 20 times the normal cross

TABLE IX. Value of R_0 for ^{24}Na computed by the MC procedure for various values of the input parameters.

T_p (MeV)	P_b	P_p	R_0 (0.9A GeV)	R_0 (1.8A GeV)
120	0.05	0.50	1.09	1.10
120	0.30	0.50	1.10	1.12
120	0.75	0.50	1.12	1.13
120	0.30	0.10	1.08	1.09
120	0.30	0.90	1.13	1.15
200	0.30	0.50	1.12	1.18
400	0.30	0.50	1.14	1.24

TABLE X. Fractional loss (in %) of ^{24}Na activity computed by the MC procedure for various values of the input parameters: *a* outside the disc, *b* outside the guard ring.

		0.9 *A* GeV		1.8 *A* GeV	
P_p	T_p (MeV)	*a*	*b*	*a*	*b*
0.5	200	10.2	3.3	8.6	2.6
0.5	200	14.5	5.1	11.8	4.0
0.5	400	20.9	8.7	16.8	6.9
0.9	400	20.9	10.8	22.4	9.6
0.9	800	34.1	17.1	29.0	14.9

section). Lower values of the product αf would be needed if some secondaries with $Z \leq 2$ also had anomalously high cross sections.

Then, in order to explain the loss at $d = 20$ cm (which, incidentally, reduces the value of R_{20} to roughly that seen at 0.9 *A* GeV) the anomalous fragments would have to revert to the ground state ("decay") during the time required to reach the "detector" disk in the $d = 20$ cm configuration. This would require (in order to have, say, 80–95 % decay)

$$d \sim (2-3)\tau\gamma \ , \tag{47}$$

where τ is the assumed proper lifetime and γ the Lorentz factor (which at 1.8 *A* GeV beam energy is about 3). For $d = 20$ cm this leads to values of τ of the order of 10^{-10} s.

It is interesting to note that the emulsion results of Ref. 1 required a similar value for the product αf. Low values of α (a few %) require very large f, hence "highly anomalous" cross sections, whereas, say, $\alpha \simeq 1$ (for PF's of $Z \geq 3$) requires the anomalous fragments to decay with $\tau \simeq 10^{-11}$ s.[22]

This latter possibility was excluded by an experiment,[8] in which the possible decay of PF's with anomalously high cross sections produced in the interaction of 1.7 *A* GeV ^{56}Fe ions with copper was investigated by means of a comparison of PF's production in "dense" and in "diluted" targets (with "decay" paths of $\simeq 2$ cm). This experiment was sensitive to anomalous fragments with $Z \geq 5$ and $\tau \simeq 10^{-11}$ s, emitted at angles $< 1°$ to the beam direction. No evidence of decay was observed and it was concluded that the data were consistent but with no anomaly and with anomalous fragments decaying with a lifetime longer than 5×10^{-11} s. These conclusions are not inconsistent with the results of the present study where "decay" paths larger by an order of magnitude were used.

The emulsion experiments[1] (as well as those performed with plastic track detectors[2,3]) were, by their very nature, unable to resolve the $\alpha \leftrightarrow f$ ambiguity. It should be recalled that our experiment is sensitive to *all* PF's ($Z \geq 1$ as well as neutrons), while *all* other experiments were sensitive to charged secondaries only, with most of them requiring $Z \geq 3$.

One might even conjecture that anomalous cross-sections may occur among *all* PF's; then $Z = 1$ secondaries might be relatively more long lived and this could possibly account also for the rather large amount of ^{24}Na found in the guard rings at 1.8 *A* GeV.

Objects "decaying" with lifetimes of the order of $\tau \sim 10^{-10}$ s naturally bring to mind hyperfragments as possible contributors to the observed "decay" effect. However, their production cross sections are known to be low (in the microbarn range). Furthermore, though the interaction cross sections of hypernuclei are unknown, all strange particle interaction cross sections are known to be lower than those for nonstrange hadrons and hence hypernuclei can hardly contribute significantly to changes in R_d.

Obviously, no anomalously high cross-sections need be invoked in order to account for the decrease of R_d at the higher beam energy if large transverse momentum secondaries are responsible for the loss at $d = 20$ cm. However, it is hard to image that reactions in Cu, integrated over *all* impact parameters, should be so drastically different from those induced by the same ^{40}A beam in KCl when "central" collisions are selected through the absence of heavy projectile fragments.[21]

This problem can and should be addressed experimentally by repeating the experiment with a 2π geometry. Then, high-energy secondaries *capable of producing ^{24}Na in sizable amounts* and emitted at angles sufficiently large to miss the guard ring of the present experiment, would also be detected. Such measurements are in progress. However, the puzzling large value of R_0 at 1.8 *A* GeV (as well as the slight excess of R_0 over the MC prediction at 0.9 *A* GeV) still remain unexplained. Anomalously large total and/or partial cross sections would easily take care of this effect, but more detailed calculations of the effects of presumed anomalously large cross sections for *unstable* PF's are needed in order to understand all features of our data.

VI. CONCLUSIONS

We have observed an unusual behavior of the energetic secondaries produced in the interaction of 1.8 *A* GeV ^{40}Ar with copper but none in an identical experiment at a lower (0.9 *A* GeV) energy beam. Two effects were observed: A large value of R_0 for the production of light target residues and a decrease in R_d with increasing distance between the disks. Our calculations which were based on conventional physics and the available high-energy data fail to explain either effect. There are at least two possible explanations (or combinations thereof) based on new phenomena.

First, it is possible that energetic secondaries are abundantly emitted at wide angles, i.e., with very large transverse momentum components. However, such secondaries were not seen in appreciable numbers in a related (though not entirely comparable) experiment[21] and hence our calculations, if based on this experiment alone, fail to explain our observations.

Second, some unstable secondaries possess unusually large interaction cross sections (or at least large *partial* cross sections for the production of the light nuclear residues investigated here); then they 'decay" in flight (i.e., revert to "normal" cross sections).

Experiments are in progress to determine whether the first interpretation is the correct one.

ACKNOWLEDGMENTS

The authors are grateful to the staff and the operating crew of the Bevalac, Lawrence Berkeley Laboratory, for supplying us with excellent argon beams. Particular thanks are given to Dr. F. Lothrop. Two of us (N.T.P. and E.M.F.) acknowledge the receipt of a Senior U.S. Scientist Award from the A.v. Humboldt Foundation and the hospitality of the Kernchemie, Marburg University. The nuclear chemists from Marburg kindly acknowledge the generous hospitality of Professor G. T. Seaborg in Berkeley. We want to thank Professor R. M. Weiner (Marburg) for many stimulating discussions. This work was supported in part by the Director, Office of Energy Research, Division of Nuclear Physics of the Office of High Energy and Nuclear Physics of the U.S. Department of Energy under Contract DE-AC03-76ERO1505, DE-AC03-76SF00098, and DE-AM06-76RLO2227, by the Bundesministerium fuer Forschung und Technologie, Federal Republic of Germany, the National Research Council of Canada and the Swedish Natural Science Research Council.

APPENDIX

In order to give the reader a clear insight into the main physical picture of our experimental conditions and facts, the results presented in Sec. IV were obtained with compacted angular intervals and other approximations described therein. In addition we tried to gain an idea of the influence of these simplifications, by performing a Monte Carlo calculation, which used as input the multiplicities and angles of the secondaries of individual events recorded in the emulsion part of the present experiment which, we remind, was performed with the same beams as the radiochemical part.

The emission angles, by themselves, would be insufficient, to predict R_0, because of the energy dependence of the ^{24}Na (and similar) cross sections; hence the MC calculation proceeded with the following assumptions regarding the energy spectra of the secondaries, are as follows.

(i) All secondaries being emitted within the projectile fragmentation cone ($\theta < \theta_c$) were assigned the beam velocity. This ignores any admixture of midrapidity particles to the fragmentation cone and exaggerates ^{24}Na production, hence Q_{11} and consequently R_0.

(ii) Since all fast secondaries with $\theta > \theta_c$ have $Z=1$ they were assumed to consist of $P_p\%$ "midrapidity protons" emitted from a fireball with a temperature T_p and of $(100-P_p)\%$ pions emitted with a temperature T_π.

(iii) The cross-section values for ^{24}Na production are those of Sec. IV A 3.

(iv) Subsequent cascading of the secondaries in the two copper disks was taken into account as follows: (a) $Z=1$ secondaries were assumed to lose a fraction $\xi(\approx\frac{1}{2})$ of their kinetic energy in each subsequent collision. (b) Heavier fragments were treated with two extreme assumptions: either they suffer quasielastic collisions with negligible energy loss, or they break up (in $P_b\%$ of the cases) into $A_Z \approx 2Z$ nucleons with beam velocity, which suffer then the fate described in the preceding paragraph. With these assumptions the effect of extra-nuclear cascading was then computed by assigning to each particle of energy E an equivalent cross section:

$$\sigma_{\text{equiv}} = \sum_{j=1}^{\infty} \sigma_{p,\pi}(E\xi^{j-1}) \left[1 - e^{-x/\lambda} \sum_{k=0}^{j-1} \frac{(x/\lambda)^k}{k!} \right], \tag{A1}$$

where λ is the secondary's collision mfp. Equation (A1) follows simply from the Poisson probabilities of successive interactions. The energy E for pions and protons with $\theta > \theta_c$ was derived from the observed angle and the MC generated (Boltzmann) transverse momenta at temperatures T_π and T_p, respectively. It turned out that varying ξ between $\frac{1}{2}$ and unity made little difference to the result because the total contribution of $Z=1$ secondaries to Q_{11} and Q_{12} is small.

(v) For secondaries of type (v) as defined in Sec. IV A their attenuation in the residual thickness of disk 1 was also taken into account.

(vi) Whenever a fast $Z=1$ track was assumed to be a proton (i.e., for all shower tracks with $\theta < \theta_c$ and for $P_p\%$ of the rest) its contribution to Q_{11} and Q_{12} was doubled in order to account for fast neutrons expected to be emitted with similar angular and energy distributions.

A few results of predictions for R_0 at the two beam energies are shown in Table IX for different extreme assumptions about the characteristics of the cascade process.

The pion "temperature" T_π which enters the calculation via the mean transverse momentum ($\langle p_\perp \rangle = 2T_\pi$ for an exponential $p_\perp$ spectrum) was held at 58 MeV while proton temperatures T_p of 120,[21] 200, and 400 MeV were tried out, in order to see the influence of exaggerated assumptions. As can be seen two main results emerge almost independently of the parameters used: (g) The R_0 value for the $0.9A$ GeV beam is close to the observed one; if anything, the computed values are slightly smaller, and an absurdly high proton "temperature" would be needed in order to reach agreement with the experimental value of 1.16 ± 0.01. (b) The R_0 values computed for the $1.8A$ GeV beam are only slightly higher than those computed for $0.9A$ GeV and can in no way be raised to

the value of ~ 1.5 observed experimentally (see Fig. 4).

In Table IV the predictions were based on *all* events observed in the emulsion experiment; in other words they refer to the *average* target nucleus (thus including collision with light, i.e., C, N, or O nuclei). An exaggeration of effects expected for a pure copper target is obtained if we base the MC calculation only on (nonperipheral) collisions with heavy (Ag, Br) selected by $N_h > 8$. In this way the R_0 value can be most be raised to 1.25 assuming "normal" temperatures T_π and T_p.

[1]E. Friedlander *et al.*, Phys. Rev. Lett. **45**, 1084 (1980); Phys. Rev. C **27**, 1489 (1983), and references therein.
[2]M. L. Tincknell, P. B. Price, and S. Perlmutter, Phys. Rev. Lett. **51**, 1948 (1983).
[3]W. Heinrich *et al.*, Phys. Rev. Lett. **52**, 2402 (1984).
[4]A. P. Gasparian *et al.*, Z. Phys. A **320**, 459 (1985).
[5]P. L. Jain and G. Das, Phys. Rev. Lett. **48**, 305 (1982).
[6]P. L. Jain *et al.*, Phys. Rev. Lett. **52**, 2213 (1984).
[7]M. M. Aggarwal *et al.*, Phys. Lett. **112B**, 31 (1982)
[8]H. A. Gustafsson *et al.*, Phys. Rev. Lett. **51**, 363 (1983).
[9]J. D. Stevenson, J. A. Musser, and S. W. Barwick, Phys. Rev. Lett. **52**, 515 (1984).
[10]T. J. M. Symons *et al.*, Phys. Rev. Lett. **52**, 982 (1984).
[11]I. A. Golutvin *et al.*, JINR Rapid Communications, 5-84, p. 8-13 (1984), Joint Institute for Nuclear Research, Dubna, USSR.
[12]M. Bano *et al.*, Phys. Lett. **166B**, 453 (1986); **196B**, 255 (1987).
[13]A. G. Karev *et al.*, Joint Institute for Nuclear Research, Dubna, 1987 (to be published).
[14]W. Heinrich, Proceedings of the 7th High Energy Heavy Ion Study, Darmstadt, 1984, Gesellschaft für Schwerionenforschung Report No. 85-10, 1984.
[15]G. Dersch *et al.*, Phys. Rev. Lett. **55**, 1176 (1985).
[16]D. J. Morrissey *et al.*, Nucl. Instrum. Methods **158**, 499 (1978).
[17]G. Dersch, Dissertation, FB Physikalische Chemie, Philipps University, Marburg, 1986 (unpublished).
[18]G. Haase, Diplomarbeit, Kernchemie, Philipps University Marburg, 1986 (unpublished).
[19]J. B. Cumming, P. E. Haustein, T. J. Ruth, and G. J. Virtes, Phys. Rev. C **17**, 1632 (1978).
[20]G. D. Cole and N. T. Porile, Phys. Rev. C **25**, 244 (1982).
[21]R. Brockmann *et al.*, Phys. Rev. Lett. **53**, 2012 (1984).
[22]H. B. Barber, P. S. Freier, and C. J. Waddington, Phys. Rev. Lett. **48**, 856 (1982).

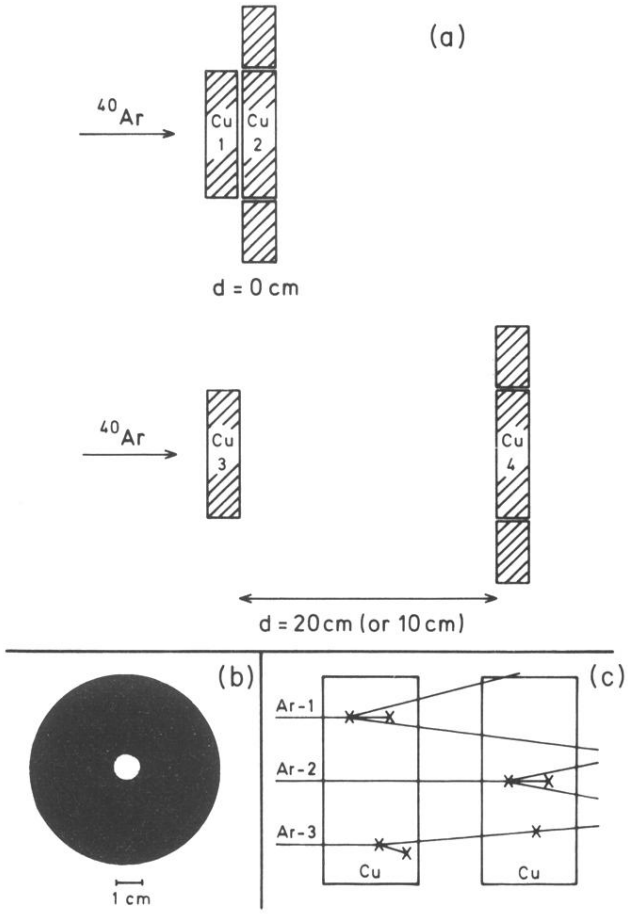

FIG. 1. (a) Schematic representation of the target setup using Cu disks and their surrounding guard rings. (b) Autoradiographic picture of a Cu disk after the irradiation. (c) Schematic representation of different reaction paths in the two Cu disks; details are given in text.